How Do Benzylic Amide [2]Catenane Rings Rotate?

ARTICLE *in* JOURNAL OF THE AMERICAN CHEMICAL SOCIETY · MARCH 1999

Impact Factor: 12.11 · DOI: 10.1021/ja9815273

How Do Benzylic Amide [2]Catenane Rings Rotate?

Michael S. Deleuze,*,† David A. Leigh,*,‡ and Francesco Zerbetto*,§

Contribution from the Departement SBG, Limburgs Universitair Centrum, Universitaire Campus, B3590 Diepenbeek, Belgium, Centre for Supramolecular and Macromolecular Chemistry, Department of Chemistry, University of Warwick, Coventry CV4 7AL, United Kingdom, and Dipartimento di Chimica "G. Ciamician", Università degli Studi di Bologna, Via F. Selmi 2, I40126 Bologna, Italy

Received May 4, 1998. Revised Manuscript Received October 26, 1998

Abstract: The structure and dynamics of three benzylic amide catenanes have been investigated using molecular mechanics and calculations employing unimolecular reaction rate theory. The study provides the first complete theoretical description of the lowest energy pathway for the circumrotation of macrocycles in a catenane system. The process is a concerted sequence of several large-amplitude motions which involve rearrangements to minimize steric and electrostatic interactions via the interplay of hydrogen bonding, formation of π-stacks, phenyl−phenyl T-shaped interactions, and amide rotamer interconversions. In spite of this complexity, unifying features are found for the description of the passing of successive moieties through the macrocyclic cavities. Analysis of the structural characteristics of transition states located along the circumrotational pathway of the three catenanes (bearing phenyl-, pyridyl-, and thiophenyl-1,3-dicarbonyl groups) furnishes a simple mechanistic interpretation of the large variation of the dynamical behavior observed in temperature-dependent NMR experiments. Calculations of the rate constants provide the ultimate insight into the complicated dynamics of these molecules, showing that the rate-determining steps do *not* necessarily correspond to the passage of the bulkiest groups and that, like a cog or rotor system, rotation of one macrocyclic ring induces, or makes easier, rotation of the other.

Introduction

The pioneering work of Sauvage, Stoddart, and others on mechanically interlocked molecules[1] has ignited interest in the development and characterization of catenanes and rotaxane systems both as key components in the development of nanoscale devices[2] and as intermediates in the synthesis of difficult or otherwise impossible to obtain synthetic targets.[3] An example of the high structural versatility that can be achieved in interlocked systems is provided by the class of benzylic amide catenanes,[4−6] serendipitously discovered[4] during the preparation of a macrocycle-based receptor for CO_2. In contrast to the co-conformationally[7] locked amide catenanes synthesized by Hunter[1e] and Vögtle,[1f] benzylic amide catenanes show unambiguous evidence[4−6] for the spinning of the interlocked macrocycles about one another in solution. Their remarkably tolerant synthesis affords ready access to derivatives with differing interring interactions[5] allowing fine-tuning of catenanes dynamic properties through the calibrated variation of electronic and steric factors.[8] Significantly, circumrotational motions (complete rotation of one macrocyclic ring through the other) can be altered and their rate constants controlled by variations of the solvent polarity which affects the complex internal networks of hydrogen bonds.[9]

While the large number of synthetic strategies for the preparation of catenanes has burgeoned[1] into many examples based on $\pi-\pi$ interactions, cation templation, hydrophobic forces, and hydrogen bonds, a thorough theoretical analysis of the dynamics of an interlocked ring system has yet to be reported.[10] A detailed understanding of the factors that govern

† Limburgs Universitair Centrum.

‡ University of Warwick.

§ Università degli Studi di Bologna.

(1) Schill, G. *Catenanes, Rotaxanes and Knots*; Academic Press: New York, 1971. (b) Sauvage, J.-P. *Acc. Chem. Res.* **1990**, *23*, 312−327. (c) Amabilino, D. B.; Stoddart, J. F. *Chem. Rev.* **1995**, *95*, 2725−2828. (d) Gibson, H. W.; Bheda, M. C.; Engen, P. T. *Prog. Polym. Sci.* **1994**, *19*, 843−945. (e) Hunter, C. A. *J. Am. Chem. Soc.* **1992**, *114*, 5303−5311. (f) Vögtle, F.; Dunnwald, T.; Schmidt, T. *Acc. Chem. Res.* **1996**, *29*, 451−460. (g) For an example of this type of catenane where the rings can rotate, see: Baumann, S.; Jager, R.; Ahuis, F.; Kray, B.; Vögtle, F. *Leibigs A. Rec.* **1977**, 761−766. (h) Gruter, J. G. M.;de Kanter, F. J. J.; Markies, P. R.; Nomoto, T.; Akkermann, O. S.; Bickelhaupt, F. *J. Am. Chem. Soc.* **1992**, *115*, 12179. (i) Fujita, M.; Ibukuro, F.; Hagihara, H.; Oguar, K.; *Nature* **1994**, *367*, 720−723. (j) Hamilton, D. G.; Sanders, J. K. M.; Davies, J. E.; Clegg, W.; Teat, S. J. *Chem. Commun.* **1997**, 897−898.

(2) (a) Whitesides, G. M.; Mathias, J. P.; Seto, C. T. *Science* **1991**, *254*, 1312−1319. (b) Bissell, R. A.; Stoddart, J. F. In *Computations for the Nano-Scale*; Blöchl, P. E., Fisher, A. J.,Joachim, C., Eds.; NATO ASI Series 240; Kluwer; Dordrecht, 1993; pp 141−152. (b) Drexler, K. E. *Annu. Rev. Biophys. Biomol. Struct.* **1994**, *23*, 377−405. (d) Anelli, P.-L.; Asakawa, M.; Ashton, P. R.; Bissell, R. A.; Clavier, G.; Górski, R.; Kaifer, A. E.; Langford, S. J.; Mattersteig, G.; Menzer, S.; Philp, D.; Slawin, A. M. Z.; Spencer, N.; Stoddart, J. F.; Tolley, M. S.; Williams, D. J. *Chem. Eur. J.* **1997**, *3*, 1113−1135.

(3) (a) Amabilino, D. B.; Ashton, P. R.; Brown, C. L.; Córdova, E.; Godinez, L. A.; Goodnow, T. T.; Kaifer, A. E; Newton, S. P.; Pietraszkiewicz, M.; Philp, D.; Raymo, F. M.; Reder, A. S.; Rutland, M. T.; Slawin, A. M. Z.; Spencer, N.; Stoddart, J. F.; Williams, D. J. *J. Am. Chem. Soc.* **1995**, *117*, 1271−1293. (b) Raymo, F. M.; Stoddart, J. F. *Pure Appl. Chem.* **1996**, *68*, 313−322. Asakawa, M.; Ashton, P. R.; Menzer, S.; Raymo, F. M.; Stoddart, J. F.; White, A. J. P.; Williams, D. J. *Chem. Eur. J.* **1996**, *2*, 877−893. (c) Johnston, A. G.; Leigh, D. A.; Murphy, A.; Smart, J. P. *Bull. Soc. Chim. Belg.* **1996**, *105*, 721−727. (d) Johnston, A. G.; Leigh, D. A.; Murphy, A.; Smart, J.P.; Deegan, M. D. *J. Am. Chem. Soc.* **1996**, *118*, 10662−10663.

(4) Johnston, A. G.; Leigh, D. A.; Pritchard, R. J.; Deegan, M. D. *Angew. Chem., Int. Ed. Engl.* **1995**, *34*, 1209−1212.

(5) Johnston, A. G.; Leigh, D. A.; Nehzat, L.; Smart, J. P.; Deegan, M. D. *Angew. Chem., Int. Ed. Engl.* **1995**, *34*, 1212−1216.

(6) Leigh, D. A.; Moody, K.; Smart, J. P.; Watson, K. J.; Slawin, A. M. *Z. Angew. Chem., Int. Ed. Engl.* **1996**, *35*, 306−310.

(7) "Co-conformation" refers to the relative positions and orientations of the mechanically interlocked components with respect to each other: Fyfe, M. C. T.; Glink, P,. T.; Menzer, S.; Stoddart, J. F.; White, A. J. P.; Williams, D. J. *Angew. Chem., Int. Ed. Engl.* **1997**, *36*, 2068−2070.

10.1021/ja9815273 CCC: $18.00
Published on Web 03/05/1999

the motion therefore remains a fascinating and crucial problem for the (computational) chemist to tackle. Such a study precedes the full, external control of the kinetics and thermodynamics of macrocyclic ring rotation, an important requirement if one is to take full advantage of interlocked architectures in practical molecular devices or if this special degree of freedom is to play a role in materials that show high orientational versatility, e.g., those based upon environment-sensitive amphiphilic catenanes.[6]

A detailed experimental investigation of circumrotation in benzylic amide catenanes is limited by both the complexity of the intricate networks of hydrogen bonds and $\pi-\pi$ interactions present and the steric constraints that exist in this class of catenanes. The X-ray crystal structure[4] of the isophthaloyl catenane, **1**, shows that complete circumvolution of one of the two macrocycles must necessarily involve some breaking of attractive inter-ring interactions (H-bonds, $\pi-\pi$ stacking, van der Waals interactions) together with transient changes in the relative positions and orientations of the two interlocked rings. Apart from the obvious alterations in the electrostatic and dispersion forces between the two macrocycles, the activation barriers and rate constants—obtained experimentally through NMR experiments[9]—are implicitly due also to intricate variations in the stretching, bending, and torsional degrees of freedom.

Here we describe a theoretical investigation of the potential energy surface (PES) of catenane **1** and its pyridyl and thiophenyl derivatives **2** and **3** (see Figure 1). Among the many simplifications used, one of the most drastic is the isolated molecules model. Its justification lies in the fact that a solvent such as $C_2D_2Cl_4$, used in ref 9, does not interact directly with the inter-ring hydrogen bond system and cannot force itself in the cavity where the major structural rearrangement occurs. Notice, however, that the influence of the solvent can become very important, as in the case of CD_3OD, when it can disrupt the inter-ring hydrogen bonds or when it can form hydrogen bonds with the catenanes. The plan of this work is to provide first a detailed survey of the conformations, co-conformations, and energy barriers involved in the lowest energy pathway for a complete circumvolution of the macrocyclic rings. Owing to the size of the molecules and the nature of the processes under investigation, the work has been carried out using molecular mechanics calculations.[11] The results are then used to characterize the dynamics of these molecules using unimolecular reaction rate theory which can be compared with available NMR data.[9]

Theory and Methodology

Overview. Specific to most interlocked molecules are low-energy dynamic processes which include both spinning, i.e., pirouetting, of a ring about a given axis and shuttling (translation) of mechanically interlocked components between two points along the catenanes or rotaxane fragment. Such motions can be referred to as circumrotational (or circumvolutional) when they involve a complete rotation of a macrocycle around the other interlocked unit. In a homocircuit catenane, i.e., one of which the two component macrocycles are identical, shuttling and pirouetting are degenerate processes, and therefore, either can describe a circumrotational action. The dynamic properties of molecules can be characterized in terms of the minimums of the PES, which correspond to locally stable conformations, and the transition states, which connect these minimums. Considering the many degrees of freedom of the systems investigated here, a complete exploration of their conformational space is clearly out of the question. Ideally, one should discard most atomic motions to retain the only one or two degrees of freedom (pirouetting, shuttling) corresponding to a circumrotational action of one of the macrocyclic rings. In practice, however, circumrotations are strongly coupled to other low-frequency motions whose effect is to minimize the energy along the circumrotational pathway. For instance, pedaling around an amide C−N bond or the torsion of one of the phenyl groups can induce the formation of π-stacks or transient T-shaped or "herringbone" interactions which can be used by the system to reduce its energy during circumrotation.

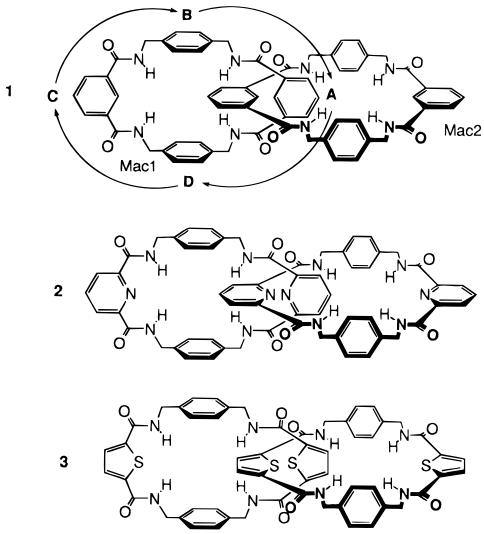

Figure 1. Chemical structure of the selected benzylic amide catenanes: isophthaloyl catenane (**1**), pyridyl catenane (**2**), and thiophenyl catenane (**3**). The rotation A → D → C → B → A describes a circumrotation of Mac1.

A possible approach to investigate the special degree of freedom of catenanes is molecular dynamics. However, circumrotational processes within the benzylic amide catenane fall in the micro- or even millisecond regime[9] and the shuttling or pirouetting would appear only as "rare events" in such calculations. To bypass this difficulty,we utilize a two-step approach that is reminescent of the procedure introduced by Stillinger and Weber for characterizing complex potential energy surfaces.[12,13] It is based on a quenching of the structures generated along a molecular dynamics trajectory to the nearest local minimum. In our approach, instead of using molecular dynamics, a representative set of starting geometries is first generated by imposing a series of rigid (uncoupled) rotations to one of the

(8) (a) For catenanes where structure variations effect circumrotational dynamics, see: Anelli, P.-L.; Ashton, P. R.; Ballardini, R.; Balzani, V.; Delgado, M.; Gandolfi, M. T.; Goodnow, T. T.; Kaifer, A. E.; Philp, D.; Pietraszkiewicz, M.; Prodi, L.; Reddington, M. V.; Slawin, A. M. Z.; Spencer, N.; Stoddart, J. P.; Vicent, C.; Williams, D. J. *J. Am. Chem. Soc.* **1992**, *114*, 193−218. (b) For catenanes where solvent variations effect circumrotational dynamics and translational isomerism, see: Ashton, P. R.; Ballardini, R.; Balzani, V.; Credi, A.; Gandolfi, M. T.; Menzer, S.; Perez-Garcia, L.; Prodi, L.; Stoddart, J. F.; Venturi, M.; White, A. J. P.; Williams, D. J. *J. Am. Chem. Soc.* **1995**, *117*, 11171−11197. (c) For electrochemically and photochemically driven macrocyclic ring motions in a catenane, see: Livoreil, A.; Sauvage, J.-P.; Armaroli, N.; Balzani, V.; Flamigni, L.; Ventura, B. *J. Am. Chem. Soc.* **1997**, *119*, 12114−12124 and references therein.

(9) Leigh, D. A.; Murphy, A.; Smart, J. P.; Deleuze, M. S.; Zerbetto, F. *J. Am. Chem. Soc.* **1998**, *120*, 6458−6467.

(10) For a recent account of a molecular modeling study of a catenane, see: Ballardini, R.; Balzani, V.; Credi, A.; Brown, C. L.; Gillard, R. E.; Montali, M.; Philp, D.; Stoddart, J. F.; Venturi, M.; White, A. J. P.; Williams, B. J.; Williams, D. J. *J. Am. Chem. Soc.* **1997**, *119*, 12503−12513.

(11) Burkert, U.; Allinger, N. L. *Molecular Mechanics*; American Chemical Society: Washington, DC, 1982; Chapter 3.

(12) Stillinger, F. H.; Weber, T. A. *J. Phys. Chem.* **1983**, *87*, 2833−2840.

(13) Stillinger, F. H.; Weber, T. A. *Science* **1984**, *225*, 983−989.

two macrocycles in a selected reference structure. Local distortions neglected in this first step are recovered by the subsequent relaxation to the closest minimum or transition state, using a truncated Newton nonlinear optimization procedure.[14]

As described in more detail below, a two-dimensional exploration of the potential energy surface was performed to describe both shuttling and pirouetting actions, thus mimicking macrocycle circumrotation in the catenanes. In practice, imposition of this rigid rotation protocol provides a host of structures whose optimization ends in one of several attractors,[15] in direct analogy with waters flowing into hydrogeographic "basins". The basins are delimited by energy barriers that are due to the constraints encountered during the circumrotation of the macrocycle. They can also be regarded as the portions of the conformational and co-conformational space that, after geometry optimization, yield the key intermediate structures along the minimum energy circumrotational pathway.

The same approach wa used to locate transition states as first-order saddle points in the potential energy surface. The optimization procedure leads successfully to transition states only when applied to initial structures already falling in the vicinity of saddle points and requires in practice the generation of several hundred initial geometries to locate only a few tens of acceptable solutions. Such an approach is nowadays justified by the low computational cost of molecular mechanics and the tremendous advances in computer processing speed realized over the last decade. The procedure was adopted after many failed attempts using the more traditional synchronous-transit method,[16] which appears much too demanding and not entirely satisfactory for benzylic amide catenane systems whose complexity prevents easy interpolation between local energy minimums. As a further bonus, the procedure based on building a rigid rotation chart also enables a reasonably systematic, and thereby controllable, exploration of the transition states along the circumrotational pathway.

One of the roughest approximations of the present modeling is that of the isolated molecule, whereas the experimental data were measured in solution.[9] Future work will have to take into account the effect of solvents, especially those able to disrupt the intramolecular hydrogen-bonding framework. It was, however, thought, and this turned out to be the case, that our simulations could be compared with the results in solvents such as $C_2D_2Cl_4$ whose effect on the H-bonds was small.

Rigid Rotation (RR) Algorithm. The generation of the molecular structures proceeds via the following sequence (see Figure 2): first an average plane for one of the two macrocycles is defined as the plane perpendicular to the largest component of its irreducible (diagonalized) inertia tensor. A first series of rotations (R_1 in Figure 2a), by an angle θ, is then applied in that plane while keeping the other macrocycle fixed. For the sake of enhanced flexibility and to improve on the description of the shuttling action, a second series of rotations (R_2) is applied, by an angle θ, about the axis of the second largest component of the inertia tensor.

To avoid generation of overly crowded, physically unsound, structures, a series of small translations of 0.01 Å is then applied iteratively (Figure 2b) to the coordinates of the rotated macrocycle. The aim is to avoid large overlaps of van der Waals spheres between atoms that are not connected, to release strong interatomic repulsive interactions, and to direct the exploration

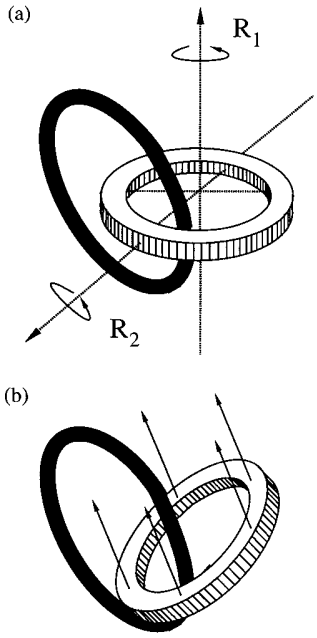

Figure 2. Representation of spinning and shuttling of the macrocycles produced by the rigid rotation algorithm: spinning [see (a)] is enforced by rotations (R_1) of a macrocycle within its average plane. Shuttling of this macrocycle along the thread of the other macrocycle is generated by rotations (R_2) about the axis of the second component of the inertia tensor (polar angle ϕ) combined with an iterative series of translations [see (b)] which minimize the steric constraints between the two macrocycles.

of the potential energy surface toward the region of the circumrotational pathways. Spinning is fully accounted for by the $R_1(\theta)$ while shuttling is effectively generated by the combination of these motions with $R_2(\phi)$. The approach affords also simple identification of possibly physically unsound situations such as accidental interlocking of the phenyl rings which ironically generates a very small catenene. At each step during the iteration of the translations, a displacement vector is calculated as a linear combination of the vectors that connect the atoms that have accidentally come too close, with, as weight coefficients, a factor that increases quadratically with the strength of the overlap. The structure is rejected if too strong overlaps still remain after many—that is 200—translations. This value was obtained by trial and error: 200 rigid translations of 0.01 Å are sufficient to identify unsound structures and release overcrowded configurations within the cavity of the fixed macrocycle, the dimensions of which do not exceed a few angstroms.

In the final stage, the procedure also checks for the "accidental" dissociation of the catenane into two unthreaded macrocycles during this operation by maximizing—in a similar iterative series of translations of 0.20 Å—the interatomic distances between the centers of mass of the two macrocycles. The manoeuvre always ends either with a locking of the translation, confirming the threaded nature of the system, or in a free uniform linear motion, indicating dissociation of the catenane structure which is then rejected. The rigidity rotated catenane structures that resist the dissociation test and successfully get through the release of strong atomic repulsions provide the initial structures used in the search of local energy minimums and saddle points.

For convenience in the following discussion, it is best to assume that once the circumrotation action has started one can discriminate momentarily between the two macrocycles and

(14) Ponder, H. W.; Richards, F. M. *J. Comput. Chem.* **1987**, *8*, 1016—1024.
(15) Becker, O. M.; Karplus, M. *J. Chem. Phys.* **1997**, *106*, 1495—5311.
(16) Halgren, T. A.; Lipsomb, W. N. *Chem. Phys. Lett.* **1977**, *49*, 222—232.

Table 1. Additional Bending Parameters for MM3

angle	k_s	l_0	$l_0{}^c$
$C_{sp2}-C_{sp3}-N_{sp2}$	1.045	110.74	0.0
$C_{sp2}(C{=}O)-C_{sp2}-N_{sp2}$(Pyr)	0.43	120.0	123.5
$C_{sp2}(C{=}O)-C_{sp2}-$S(Thio)	0.38	119.0	0.0

therefore assign different labels to them. The rigidedly rotated macrocycle is therefore referred to as Mac1 and the fixed one, Mac2 (Figure 1).

Selected Force Field: MM3. MM3 is one of the most complete and general force fields provided by Allinger's group for molecular mechanics computations.[17−19] Its efficiency and accuracy has been assessed on a wide range of organic compounds and can be compared against results obtained using an improved force field (MM4) for saturated hydrocarbons.[20] In addition to calculations of heats of formation and structural results in the gas phase and crystals, the MM3 force field has been constructed[21] to fit other experimental data, such as rotational barriers and steric energies in cyclic and cage structures.[22] as well as vibrational spectra and properties that depend on the vibrational levels (entropies and specific heats).[18] For instance, the experimental rotational barriers in congested hydrocarbons were reproduced with an absolute and average accuracy of $\Delta(\Delta G^{\ddagger}) = 1.02$ kcal/mol or 7.9%. Most importantly for the present purpose, MM3 also includes specific interatomic nonbonded potential energy functions[19] that allow a quantitative treatment of the van der Waals and electrostatic interactions which play an essential role in hydrogen bonding and in the $\pi-\pi$ interactions between aromatic rings.[21,22] As a further example, MM3 was used to investigate crystal packing of benzene, byphenyl, and hexamethylbenzene molecules. The calculated and (experimental) heats of sublimation were found to compare very nicely: 10.92 (10.42), 18.26 (19.50 ± 0.5), and 16.83 (17.86 ± 0.5) kcal/mol.[19]

The MM3 results presented here have been obtained using a recent and slightly adapted version of the TINKER package.[23−25] The treatment includes specific contributions for the out-of-plane deformations of aromatic rings, together with a π-SCF treatment of the conjugated segments and of their changes, bond lengths, and stretching force constants. A few additional parameters, interpolated from existing parameters, had to be supplied (Tables 1 and 2) to describe the bending and torsional energy contributions arising from conjugated amides.

It is worth emphasizing that the major factors that govern the circumrotation processes are the π-interactions and hydrogen bonds linking the two macrocycles. It should also be noticed that the eight phenyls and the rather small macrocyclic cavity make the rings quite rigid, a feature that can contribute to decrease the sensitivity of the results to the details of the potential, in particular the high-order anharmonic corrections of torsions. The comparison of the calculated barriers and rate constants against experiment can be used to vouch, a posteriori, for the accuracy of the model.

Table 2. Additional Torsional Parameters for MM3

dihedral angle	V_1	V_2	V_3
$C_{sp2}-C_{sp3}-N_{sp2}-H$	0.0	0.0	0.3
$C_{sp2}-C_{sp3}-N_{sp2}-C_{sp2}(C{=}O)$	−3.0	0.0	0.3
$N_{sp2}-C_{sp3}-C_{sp2}-C_{sp2}$	0.0	0.0	0.0
$C_{sp2}-C_{sp2}(C{=}O)-N_{sp2}-H$	0.0	3.8	0.0
N_{sp2}(Pyr)$-C_{sp2}-C_{sp2}(C{=}O)-O$	0.3	8.0	0.0
N_{sp2}(Pyr)$-C_{sp2}-C_{sp2}(C{=}O)-N_{sp2}$	0.0	1.5	0.0
$C_{sp2}-N_{sp2}$(Pyr)$-C_{sp2}-C_{sp2}(C{=}O)$	0.0	15.0	0.0
S(Thi)$-C_{sp2}-C_{sp2}(C{=}O)-O$	0.8	15.0	2.6
S(Thi)$-C_{sp2}-C_{sp2}(C{=}O)-N_{sp2}$	0.8	11.0	0.8
$C_{sp2}-$S(Thi)$-C_{sp2}-C_{sp2}(C{=}O)$	0.0	1.7	0.4

Characterization of Transition States. The characterization of transition states amounts to the analysis of the Hessian matrix, **F**, in terms of its eigenvalues:

$$\mathbf{FL} = \Lambda\mathbf{L} \tag{1}$$

where the individual elements of the Hessian are defined as

$$F_{ij} = \partial^2 V/\partial q_i \partial q_i \tag{2}$$

with $q_i = m_i^{1/2} x_i$.

Solution of eq 1 yields the normal modes of vibration L_i and the related frequencies:

$$\nu_i = \sqrt{\lambda_i/4\pi^2 c^2} \tag{3}$$

Each transition state has one negative Hessian eigenvalue λ_i, which implies one imaginary frequency ν_i. The associated normal mode of vibration provides infinitesimal mass-weighted atomic displacement vectors, $\mathbf{Q} = \mathbf{L}^{\dagger}\mathbf{q}$. Such vectors correspond to the atomic motions that initiate the return of a transition stage to the closest local energy minimums, which are easily identified by slightly distorting the transition-stage geometry along the eigenvector and relaxing this structure on both sides of the saddle point. By comparison of the energies and geometries obtained (e.g., using as a quantitative criterion the root-mean-square difference between atomic positions), it is then possible to assemble these structures along a global energy profile for the circumrotation, from which one can derive energy barriers and calculate kinetic rate constants. For a better characterization, one can also calculate the effective mass involved in the transition and the related effective force constant, using

$$M^* = 1/\sum_i (m_i^{-1/2} L_i)^2 \tag{4}$$

which represents an average of atomic masses with atomic displacements as weight factors, and

$$K^* = 4\pi^2 \nu_i^2 M^* \tag{5}$$

Calculation of Kinetic Rate Constants. Macroscopic rate constants for molecular rearrangements can be calculated, in the context of transition-state theory,[26−28] as

(17) Allinger, N. L.; Yuh, Y. H.; Lii, J.-H. *J. Chem. Soc.* **1989**, *111*, 8551−8566.
(18) Lii, J.-H.; Allinger, N. L. *J. Am. Chem. Soc.* **1989**, *111*, 8566−8575.
(19) Lii, J.-H.; Allinger, N. L. *J. Am. Chem. Soc.* **1989**, *111*, 8576−8582.
(20) Allinger, N. L.; Chen, K.; Lii, J.-H. *J. Comput. Chem.* **1996**, *17*, 642−668.
(21) Patterson, I.; Liljefors, T. *J. Comput. Chem.* **1987**, *8*, 1139−1145.
(22) Allinger, N. L.; Lii, J.-H. *J. Comput. Chem.* **1987**, *8*, 1146−1153.
(23) Ponder, J.; Richards, F. *J. Comput. Chem.* **1987**, *8*, 1016−1024.
(24) Kundrot, C.; Ponder, J.; Richards, F. *J. Comput. Chem.* **1991**, *12*, 402−409.
(25) Dudek, M. J.; Ponder, J. *J. Comput. Chem.* **1995**, *16*, 791−816.
(26) Gilbert, R. G.; Smith, S. C. *Theory of Unimolecular and Recombination Reactions*; Blackwell Scientific Publications: Oxford, 1990.
(27) Pilling, M. J.; Seakins, P. W. *Reaction Kinetics*; Oxford University Press: Oxford, 1995.
(28) (a) Baer, T.; Hase, W. L. *Unimolecular Reaction Dynamics, Theory, annd Experiment*; Oxford University Press: Oxford, 1996. Steinfeld, J. I.; Francisco, J. S.; Hase, W. L. *Chemical Kinetics and Dynamics*; Prentice Hall: Englewood Clifts; NJ, 1998.

$$k(T) = \frac{k_B T}{h} \frac{Q^{\ddagger}}{Q} e^{-E_0/k_B T} \quad (6)$$

This equation is derived in the context of unimolecular reaction theory[26−28] under the ergodicity hypothesis, which is equivalent to the requirement of rapid energy randomization throughout the vibrational normal modes on the time scale of the rearrangement, and invoking the high-pressure limit for energy thermalization via Boltzmann averaging. The circumrotation of catenanes in solution represents an ideal case for the application of this approach, if one considers the numerous degrees of freedom of these systems and the time scale of the motions involved.

In the actual calculations reported in this work, eq 6 uses vibrational partition functions of the minimum, Q, and of the transition state, $Q^{\ddagger}$. These are evaluated in the harmonic approximation, using

$$Q = \prod_i (1 - e^{-\hbar\omega_i/k_B T})^{-1} \quad (7)$$

In all calculations, activation energies obtained from MM3 calculations were corrected for zero-point vibrational effects. More sophisticated approaches to the calculations of rate constants are available.[29] However, the success obtained by the present treatment made us refrain from complicating even further an already complex scenario.

Simulated Annealing. In order to identify in a specific manner the most stable structure among all the many energy minimums of the catenanes, molecular dynamics simulated annealing calculations were performed using the velocity Verlet integration method and a time step of 0.25 fs for updating trajectories. Annealing was implemented via the Groningen method[30] with a coupling to an external bath at 800 °C, considering 1000 dynamic steps for thermal equilibration. The cooling phase was performed in 8000 steps, using a sigmoidal scaling of temperature.

Results and Discussion

Isophthaloyl Catenane 1. (a) X-ray Structure versus Global Minimum. The first problem that needed to be addressed in the study of the intricate dynamics of such large systems arises from the definition of suitable reference structures both as starting points for the motion itself and for the definition of the origin of the energy scale.

In the first series of calculations on catenane **1**, the structure used in the rigid rotation algorithm was generated by relaxing the X-ray diffraction solid-state structure into the closest MM3 energy minimum. In the relaxed structure (XRD, Figure 3a), both macrocycles adopt a chair conformation and can be considered as essentially equivalent (they are equivalent in the actual crystal structure). The arrangement has six intermacrocycle hydrogen bonds, four of which derive from two bifurcated bonds, and a series of π-interactions which involve four phenyl rings that form two pairs of slightly tilted stacks. The main characteristics of the XRD structure are its mostly planar, elongated character, which favors the development of intermolecular hydrogen bonds and a number of $\pi-\pi$ interactions in the solid state.[4] Aside from this choice of reference, simulated annealing calculations were performed to locate the most stable structure in the gas phas. It was found that the global energy minimum, GEM (Figure 3b), is 4.3 kcal/mol lower than the XRD structure. In the GEM structure, one of the macrocycles lies in a boat conformation, while the other still displays a chair form. This makes for a more globular conformation, which enhances the role played by internal, weakly binding forces. It can be characterized as having three sets of bifurcated hydrogen bonds and three parallel-displaced π-stacks. As a result of the more strained character of the global energy minimum, the inclusion of the entropy, calculated using the harmonic frequencies, reduces the energy difference between the XRD and the GEM structures to 1.72 kcal/mol at room temperature. This small energy difference could easily be reverted by interactions with the environment. Preliminary investigations on these two co-conformers embedded in random distributions of 58 $C_2H_2Cl_4$ molecules show that the XRD structure is in average ∼3 kcal/mol more stable than the vacuum GEM structure. Importantly, it is known in the case of proteins that the lack of solvent tends to favor more globular structures.[31] From the Connoly exclusions volumes evaluated with a probe of 2.8-Å radius, an acceptable size in comparison with that of $C_2H_2Cl_4$, the XRD form appears also more compact by 56.3 Å^3. This slight but significant reduction (−1.2%) of the exclusion volume (∼4600 Å^3) should mean an additional stabilization of the XRD form by a few tenths of a kilocalorie per mole in the liquid phase. We plan to address the role of solvents in a future report. Here, we have considered both structures, although as it will become apparent later, the energetics of the XRD structure closely follow that observed experimentally in $C_2H_2Cl_4$.

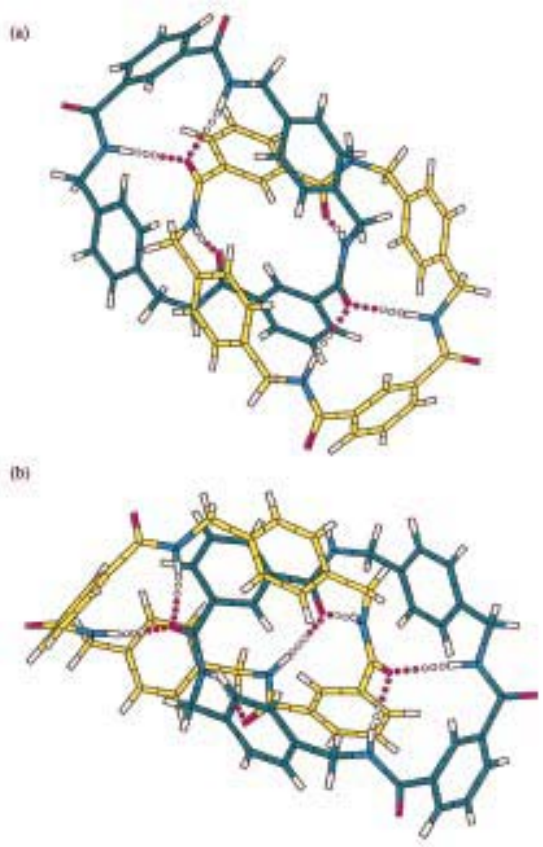

Figure 3. Optimized structures of catenane **1**: (a) XRD structure produced by relaxation from the X-ray diffraction data (selected reference); (b) global energy minimum, GEM.

(29) Truhlar, D. G.; Garrett, B. C.; Klippensteing, S. J. *J. Phys. Chem.* **1996**, *100*, 12771−12800 and references therein.

(30) Berendsen, H. J. C.; Postma, J. P. M.; van Gusteren, W. F.; DiNola, A.; Haak, J. R. *J. Chem. Phys.* **1984**, *81*, 3684−3690.

(31) Steinbach, P. J.; Brooks, B. R. *Proc. Natl. Acad. Sci. U.S.A.* **1993**, *90*, 9135.

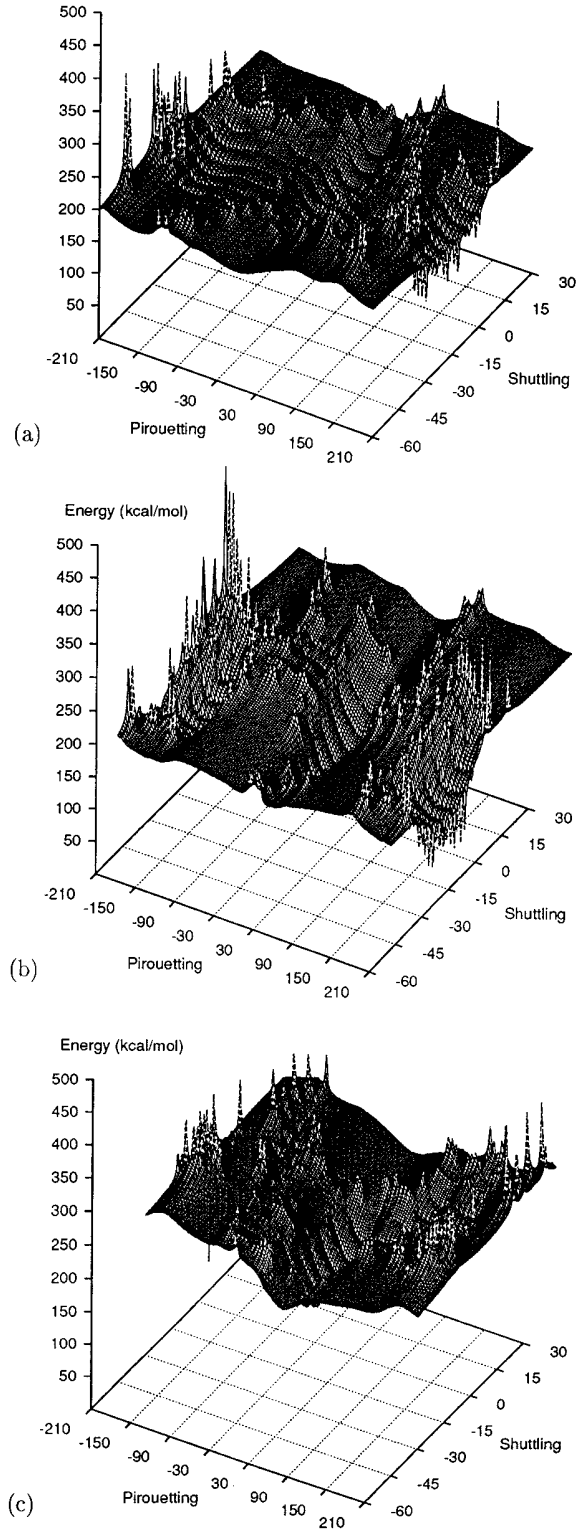

Figure 4. Rigid rotation charts (MM3 energy at the first iteration versus rotation angles, θ and ϕ) of catenane **1** for (a) one of the macrocycles within the XRD structure and for the macrocycles in (b) boat and (c) chair forms within the GEM structure.

(b) Rigid Rotation Charts. A series of 1280 rotations ($-180° \leq \theta \leq 180°$; $-90° \leq \phi \leq 30°$, with steps of 6°) were used to construct the RR charts of the XRD (Figure 4a) and GEM (Figure 4b and c) structures. For the GEM structure, the rigid circumvolution of both macrocycles had to be applied since they are nonequivalent.

A total of 767 suitable structures were obtained using the RR algorithm in conjunction with the XRD structure. From their energies, these structures define large conformational basins (Figure 4a), extending nicely in both the equatorial (θ) and polar (ϕ) directions. This is taken to indicate that the XRD structure provides abundant freedom for pirouetting of one the macrocycles (Mac1) or for shuttling of the other macrocycle (Mac2). Four major barriers can be identified in the energy chart, located at $\theta = -40°$, $\theta = -120°$, $\theta = 150°$, and $\theta = 60°$ and, in a zeroth-order picture, correspond to the passing of the bulkiest groups of Mac1 through the cavity of Mac2 (successively: (i) the isophthaloyl unit A, (ii) the 1,4-xylylene unit B, (iii) the isophthaloyl unit C, and (iv) the 1,4-xylylene unit D, Figure 1).

The RR algorithm generated slightly less prospective structures for the circumrotation of the boat and chair macrocycles of the GEM structure (671 and 666, respectively). In both cases, the GEM reference falls inside a deep, narrow canyon, surrounded by huge and steep energy barriers. It therefore shows a much more pronounced aversion for circumrotation. From inspection of the general aspects of the rigid rotation charts, the global energy minimum appears much less suited than the XRD structure as a starting point for "launching" circumvolutions. Significantly, from the energy scale of these charts, ranging over several hundreds of kilocalories per mole, it is also obvious that the minimum energy circumvolutional pathway for **1** must be by far more complex than a simple rigid rotation mechanism.

(c) Optimized Rotation Charts. After optimization, the 767 initial geometries derived by rigid rotation of one of the two macrocycles in the XRD structure yielded 135 different local energy minimums, some of which appear to fall into a large energy plateau when displayed as a function of the equatorial rotation angle θ (Figure 5a). A first series of levels appear at $\Delta E = +5$ kcal/mol above the reference but cover only partially the rotation chart. As demonstrated below, these structures relate to some of the intermediate- and short-lived species involved in the circumrotation process. Energy must be increased up to $\Delta E = +10-12$ kcal/mol above the reference in order to ensure complete coverage of the equatorial rotations by locally stable intermediates.

As shown in Figure 5a, the GEM and XRD structures fall at two opposite sides of the circumrotation pathway ($-48° \leq \theta \leq 24°$ for XRD and $\theta = 162°$for GEM). In the series of 767 structures derived from the XRD geometry and subsequent MM3 optimizations, the global energy minimum appears only once. Correspondingly, in the optimized charts of the global energy minimum, the XRD form was obtained only 22 times out of a set of 1337 zeroth-order structures. In relation to the conclusions drawn by applying the rigid rotation algorithm, the GEM structure appears to have as close neighbors (see the optimized charts of Figure 5b and c) structures of much higher energy. This is particularly evident when considering the circumrotation of the macrocycle in the chair conformation (Figure 5c). In this case, the internal energy needs to be increased by at least 20 kcal/mol in order to provide complete coverage of the circumrotation path by stable intermediates. Clearly, the GEM structure is not well suited as a starting point for a low-energy circumrotational process.

Taking the XRD structure as the global reference, any rearrangement leading to the global minimum should therefore be basically regarded as a dead end. If one assumes that the global energy minimum provides the dominant structure in a nonpolar solvent (which is probably not the case, although this

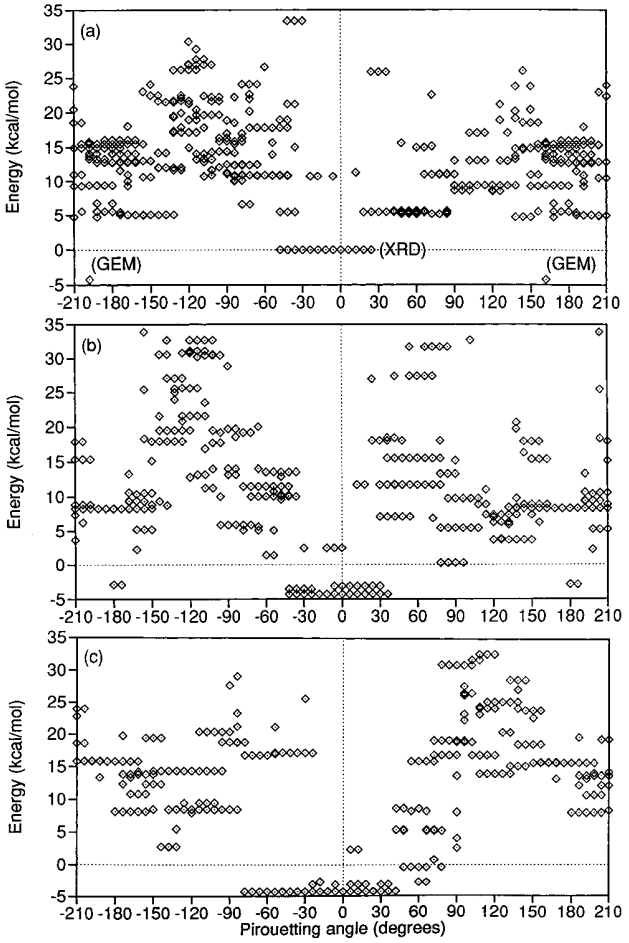

Figure 5. Optimized rotation charts (final MM3 value for the total energy versus the equatorial rotation angle θ) of catenane **1** for (a) one of the macrocycles within the XRD structure and for the macrocycles in (b) boat and (c) chair forms within the GEM structure.

is a question that may be open to debate), a major issue to address would be the location of a suitable pathway (with a low $\Delta G^{\ddagger}$ since it is not observed[9] by NMR) that connects the GEM and the XRD forms, in which circumrotation can occur more easily.

Hydrogen bonds are a key component for understanding the nature of the co-conformational distributions outlined for catenane **1** in Figure 5. In Figure 6, the energy of all the identical local minimums and transition states is compared to the sum of the cubic inverse of the distances between nonbonded amide hydrogens and oxygen atoms, as a rough criterion to evaluate the strength of hydrogen bonds. In particular, for **1** in Figure 6a, there is a clear overall relationship between the energetics of the co-conformers and hydrogen bonding which can stabilize or destabilize the structures by up to 30−40 kcal/mol. The disruption of the internal networks of hydrogen bonds in a polar solvent should therefore tremendously increase the kinetics of circumrotation, an observation confirmed experimentally.[9]

(d) Transition States and Global Energy Profile. The transition states found along the circumrotation path of catenane **1** are listed in Table 3 and the structures of the most relevant ones displayed in Figure 7, together with the displacement vectors, *Q*, which describe the vibrational normal mode associated with the negative curvature. These states can be readily distinguished from other transition states corresponding to local molecular rearrangement because of their very low imaginary frequency (10−30 i cm^{-1}), a high effective mass (6.3−7.6 au),

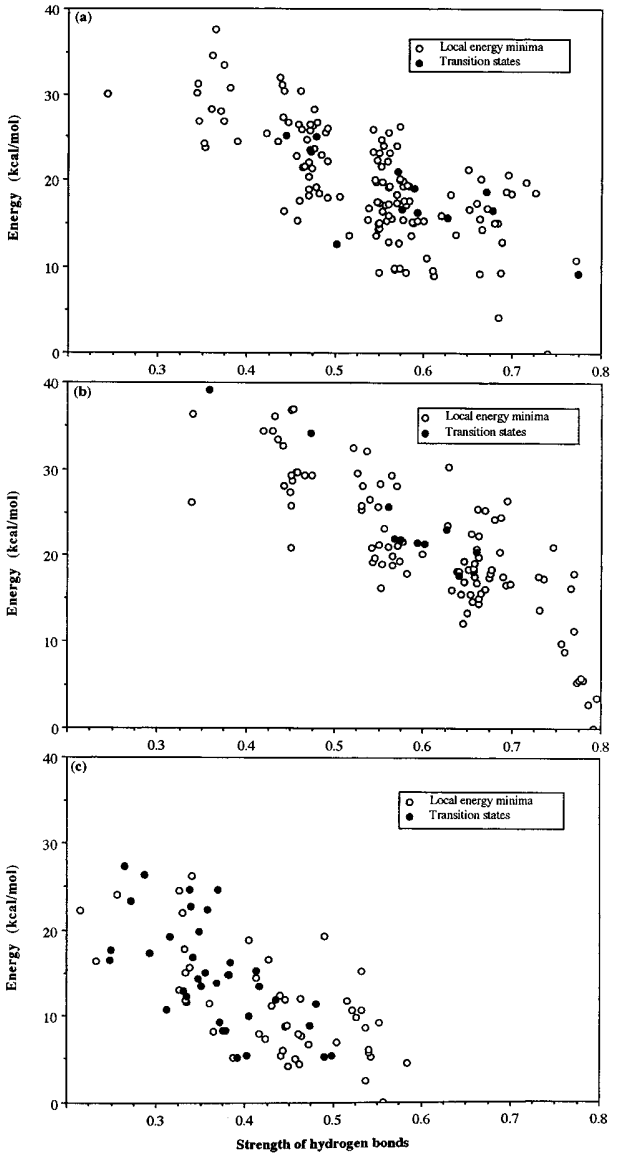

Figure 6. Dependence of the energy of the local energy minimums and transition states on the strength of hydrogen bonding for (a) **1**, (b) **2**, and (c) **3**.

and a correspondingly low effective force constant (10^{-3}−10^{-4} au cm^{-2}). Overall these quantities reflect the smooth and collective nature of these transition states. A circumvolution energy profile was constructed (Figure 8a) from the saddle points and the energy minimums which can be obtained from them. Connection between the two types of critical points was obtained using a shake-up procedure which employs the negative Hessian eigenvector. The profile was assembled by visual inspection of the molecular rearrangements, which were then ordered "chronologically" as a series of snapshots of a continuous—and rather complicated(!)—movie. In particular, when constructing this profile we considered as equivalent (Figure 8) local minimum with very similar energies and for which the mean square root of the difference of the interatomic distances is small.

The profile exhibits two major mountain ranges corresponding to the passing of the 1,4-xylylene (type I process[9]) and of the aromatic 1,3-dicarbonyl moieties (type II process[9]) of one of the macrocycles through the cavity of the other. These ranges can be further partitioned into local ridges and valleys, the succession of which reflects nicely the passing of the following

Table 3. Transition State Found along the Circumrotation Path of the Isophthaloyl-Based Catenane **1**

obsd passing[a]	$\Delta U^{\ddagger}$ (kcal/mol)	$\Delta U^{\ddagger}$ $1/2\Sigma(\Delta\omega_i)$ (kcal/mol)	$\Delta S^{\ddagger}$ (cal/(mol K))	ω (i cm^{-1})	M^*	K^*
I_a (perp) -t1	12.25	11.75	−1.78	13.56	7.28	-1.34×10^4
I_b (perp) -t2	16.76	15.63	−1.40	32.23	6.32	-6.56×10^4
I_b (perp) -t3	12.06	10.57	−6.69	19.12	7.41	-2.71×10^3
I_c (perp) -t4	13.69	12.72	+0.63	32.13	7.62	-7.87×10^4
II_a (perp) -t5	19.26	17.67	−3.50	8.85	7.10	-5.66×10^2
II_a (para) -t6	5.07	4.66	−1.08	13.07	6.69	-1.13×10^3
II_b (perp) -t7	20.78	21.58	−6.74	21.82	7.02	-3.34×10^3
II_b (para) -t8	14.39	13.72	−4.61	18.93	6.95	-2.49×10^3
II_c (perp) -t9	20.97	19.05	−6.76	21.46	7.66	-3.52×10^3
II_c (para) -t10	11.36	11.47	−4.84	3.73	6.33	-8.82×10^2
II_c (perp) -t11	8.38	8.04	−6.98	10.94	6.63	-7.92×10^2
III (perp) -t12	21.84	20.69	−2.34	24.91	7.45	-4.62×10^4
GEM → XRD -t13[b]	16.50	15.11	+9.78	18.25	6.74	-2.50×10^3
XRD → GEM -t13	12.25	10.99	−0.08	18.25	6.74	-2.50×10^3

[a] Ia, methylene unit; Ib, phenyl unit; Ic, methylene unit of the *p*-xylyl moiety; IIa, amide unit; IIb, phenyl unit; IIc, amide unit of the isophthaloyl moiety; III, ring conversion GM → XRD-like structure. [b] Taking the GEM structure as the reference in the calculations.

units: CH_2 (Ia), C_6H_4 (Ib), CH_2 (Ic), NHCO (IIa), C_6H_4 (IIb), and CONH (IIc).

The transition states that appear along the lowest energy path for the passage of the $CH_2C_6H_4CH_2$ moiety (Figure 7a−c) are all characterized by one fewer bifurcated hydrogen bond than the XRD structure. The passing *p*-xylyl fragment forms a phenyl−phenyl T-shaped complex with one of the isophthaloyl groups of the other macrocycle, an arrangement that leads us to name these transition-states "perpendicular". The breakdown of some hydrogen bonds between the two macrocycles is partially compensated for by other stabilizing interactions. For instance in TS Ib of Figure 7b, the stabilizing interactions take the form of (i) a π-electron triple decker which involves the electron-rich phenyl rings of two *p*-xylylene moieties and the electron-poor ring of one isophthaloyl unit and (ii) a herringbone π-stacking sequence involving the phenyl rings of three *p*-xylylene units. Interestingly, the successive passages of the Ia, Ib, and Ic units of Mac1 induce similar distorsions and rearrangements in Mac2 (Figure 7a−c), *indicating that the passage of the CH_2−C_6H_4−CH_2 moiety should proceed readily once it has started!* As a result of the loss of one hydrogen bond and of the enhancement of steric interactions inside the cavities, these transition states fall (Figure 8a, Table 3) at $\Delta G^{\ddagger}$ (298 K) = 12−13 kcal/mol above the selected reference (the $\Delta G^{\ddagger}$ were obtained with the inclusion of the zero-point energies and the vibrational entropy was calculated in the harmonic approximation). This result is in very good agreement with experiment ($\Delta G^{\ddagger}$ = 12.3 kcal/mol at 298 K, in $C_2D_2Cl_4$).[9]

Similar perpendicular arrangements were also found (Figure 7d,e) for the passing of one of the isophthaloyl groups of Mac1 through the cavity of Mac2. The central T-shaped phenyl−phenyl interaction this time involves the positively charged phenyl rings of two isophthaloyl units. These transitions states fall at much higher energies (19−22 kcal/mol above the reference structure) as a result of strong electrostatic repulsions.The lowest energy pathway (Figure 7f−h) for the passing of the isophthaloyl unit is, instead, found 14.4 kcal/mol above the reference (15.1 kcal/mol upon inclusion of vibrational entropy at 298 K), which compares fairly well with the energy barrier found experimentally for that passage ($\Delta G^{\ddagger}$ = 14.5 kcal/mol at 298 K, in $C_2D_2Cl_4$).[9] In this transition state (Figure 7g), the passing phenykl ring is stacked between two *p*-xylyl units in a triple-decker sandwich of aromatic rings, an arrangement that leads us to characterize this structure as "parallel". With this modality for the subunit passage, some of the transition states (Figure 7f,h) corresponding to the amide units (IIa, IIc) appear to fall at much lower energies (5.1 or 8.4 kcal/mol above the selected reference, Figure 8a).

Interestingly from the point of view of the systematics, inspection of the structures shows that when compared to the rotational action imposed with the rigid rotation algorithm the two macrocycles have exchanged their roles for the parallel passing so that the pirouetting action can be thought as due to Mac2! This seems to indicate that—as in a macroscopic rotor system[32]—*the circumrotation of one ring induces, or at least makes easier, the rotation of the other*. The crossing point for the activation of the other "rotor" is the passing of one isophthaloyl unit with its intricate rearrangement of the network of the intramolecular intermacrocycle forces. This idea of a crossing point associated with the passing of this unit is further supported by the observation that, in the corresponding transition state, the four isophthaloyl units are roughly aligned so that the roles of the macrocycles can be easily interchanged. Furthermore, tiny variations in the structure of this transition state yield very different solutions which, in a sense, describe a chaotic behavior of the catenane in the conformational region surrounding that passing and once again the possibility of role reversal.

By focusing on this region and performing further rigid rotation scans, we could identify another circumrotational transition state (Figure 7i) resembling the passing of the isophthaloyl unit in the parallel mode at slightly lower energy (12.25 kcal/mol). This transition state connects the GEM to a structure closely resembling the XRD structure. Therefore, if the GEM structure is the predominant one under nonpolar conditions, this transition state is probably the one required for the interconversion of the globular GEM conformation into a suitable starting point for the circumrotation process of catenane **1**.

(e) Rate Constants and Dynamics. As shown in the previous section, the dynamics of catenane **1** can be fairly well understood by assuming that the rate-determining steps correspond to the passage of the bulkiest phenyl units, which can occur either in the perpendicular or in the parallel passing mode. However, comparing directly the calculated activation energies to those inferred experimentally from NMR measurements may be somewhat misleading, since the density of vibrational states in the transition or reactant states could easily complicate the overall picture.

The rate constants associated with the most relevant transition states of catenane **1** are listed for different temperatures in Table

(32) Kelly, T. R.; Tellitu, I.; Sestelo, J. P. *Angew. Chem., Int. Ed. Engl.* **1997**, *36*, 1866−1868.

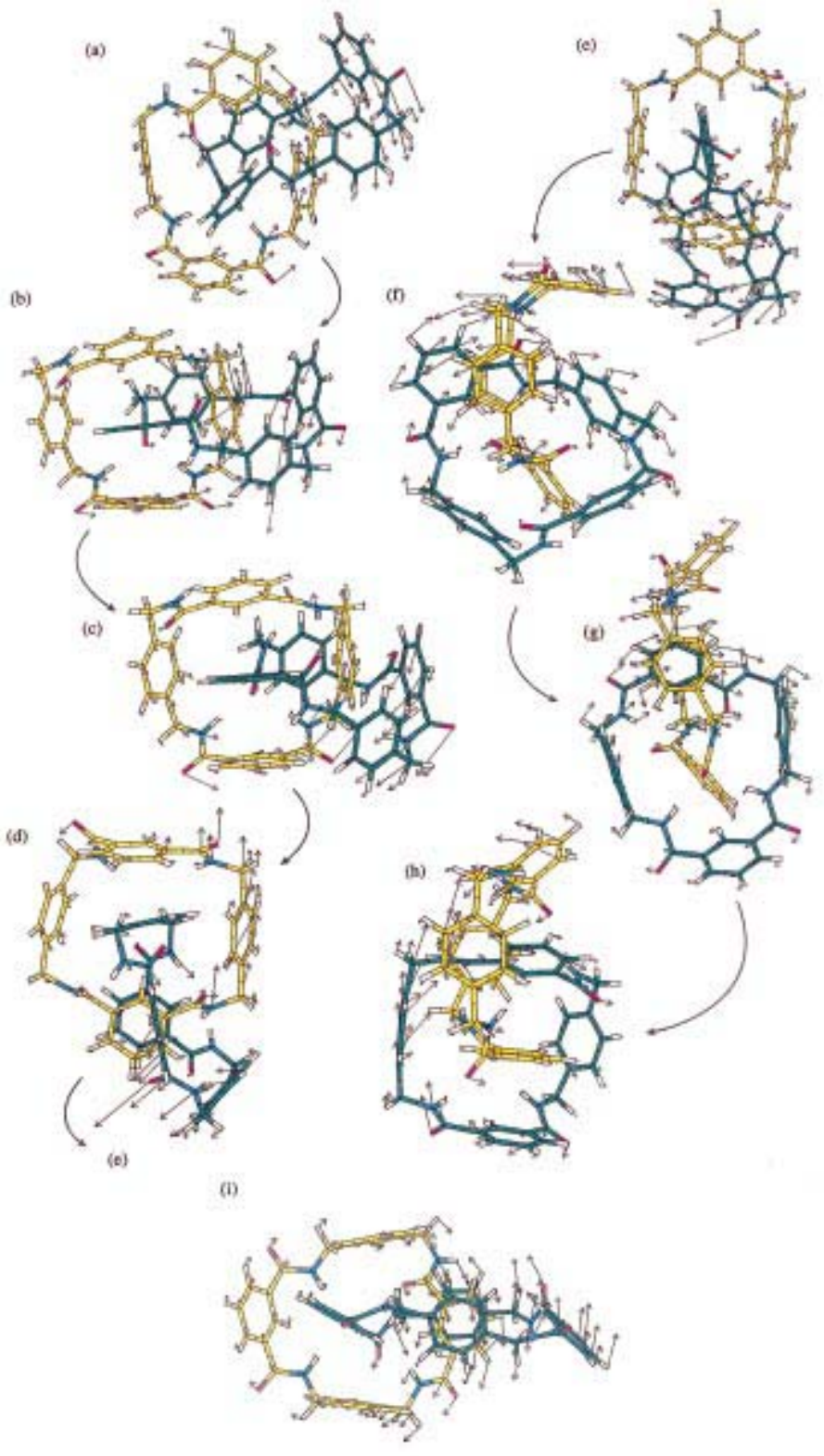

Figure 7. Transition sates along the circumrotational pathway of catenane **1** for the passing of the *p*-xylyl unit in the perpendicular mode (a−c) and the isophthaloyl unit in the perpendicular mode (d,e) and in the parallel mode (f−h). Mac1 and Mac2 are drawn in yellow and green, respectively. The structures and infinitesimal displacement vectors correspond to the following: (a) step Ia-perp (t1), first methylene group (CH_2−C_6H_4−CH_2); (b) step Ib-perp (t3), first phenyl group ($CH_2C_6H_4$−CH_2); (c) step Ic-perp (t4), second methylene group (CH_2−C_6H_4−CH_2). (d) step IIa-perp (t5), first amide group (*HNOC*−C_6H_4−CONH); (e) step IIb-perp (t7), second phenyl group (HNOC−C_6H_4−CONH); (f) step IIa-para (t6), first amide group (*HNOC*−C_6H_4−CONH); (g) step IIb-para (t8), second phenyl group (HNOC−C_6H_4−CONH); (h) step IIc-para (t10), second amide group (HNOC−C_6H_4−*CONH*). (i) transition state t13 involved in the interconversion of the XRD and GEM structures of **1**.

4. As shown neatly by these data, the rate-determining step for the passing of the 1,4-xylyl unit *does not*, in fact, correspond to the phenyl ring but to the first methylene unit, although the corresponding activation energy is slightly lower [$\Delta G^{\ddagger}$(298 K)

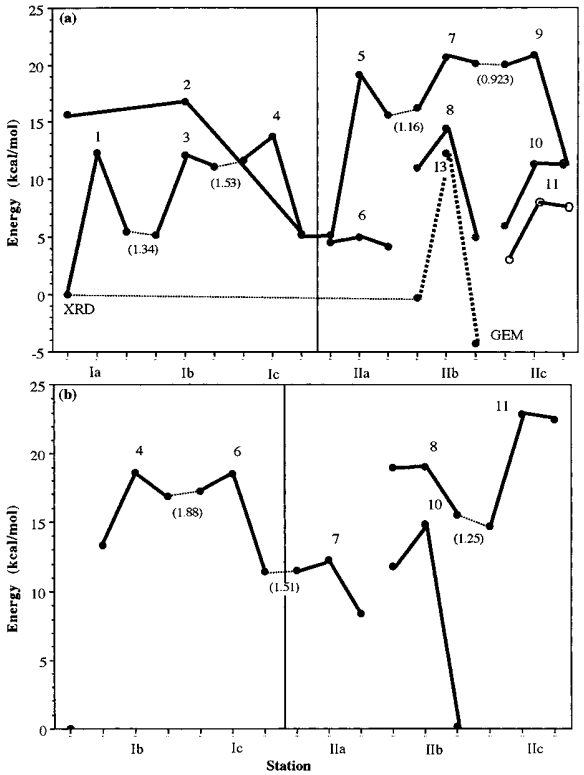

Figure 8. Global energy profile for the circumrotation of catenane **1**: step Ia, first methylene group (*CH*$_2$−C$_6$H$_4$−CH$_2$); step Ib, 1,4-substituted phenyl group (CH$_2$−*C$_6$H$_4$*−CH$_2$); step Ic, second methylene group (CH$_2$−C$_6$H$_4$−*CH$_2$*); step IIa, first amide group (*HNOC*−C$_6$H$_4$−CONH); step IIb, 1,3-substituted phenyl group (HNOC−*C$_6$H$_4$*−CONH); step IIc, second amide station (HNOC−C$_6$H$_4$−*CONH*). (b) Global energy profile for the circumrotation of catenane **2**: step Ia, first methylene group (*CH$_2$*−C$_6$H$_4$−CH$_2$)' step Ib, 1,4-substituted phenyl group (CH$_2$−*C$_6$H$_4$*−CH$_2$); step Ic, second methylene group (CH$_2$−C$_6$H$_4$−*CH$_2$*); step IIa, first amide group (*HNOC*−C$_5$NH$_3$−CONH); step IIb, pyridyl group (HNOC−*C$_5$NH$_3$*−CONH); step IIc, second amide group (HNOC−C$_5$NH$_3$−*CONH*). Values in parentheses provide the root-mean-square difference on atomic interdistances between local energy minimums. Numerical details on these transition states are provided in Tables 3−6.

= 12.28 kcal/mol instead of $\Delta G^{\ddagger}$(298 K) = 12.50 kcal/mol]. By taking into account dynamic effects, one can therefore slightly improve the agreement with the apparent energy barrier for that process found in NMR experiments [$\Delta G^{\ddagger}$ = 12.3 kcal/mol at 298 K in C$_2$D$_2$CL$_4$[9]]. These results are consistent with the idea that *the passing of the first CH$_2$ unit induces in the "passive" Mac2 the distorsions required for the subsequent passages of C$_6$H$_4$ and then CH$_2$ moieties*.

Furthermore, the passing of the amide group of one macrocycle through the cavity of the other could, in principle, be detected from their activation barrier. The $\Delta G^{\ddagger}$(298 K) = 5−8 kcal/mol leads to rates of the order of 10^9 s^{-1}. To be detected by SPT-SIR or from coalescence phenomena in NMR experiments, however, these would require temperatures around 100 K, currently beyond the range of low-temperature solution NMR experiments.

From the data displayed in Table 4, it appears that the global rate-determining step for the circumrotation of catenane **1** corresponds to the passing of the phenyl ring of the isophthaloyl unit, which has a rate constant of ∼100 s^{-1} for an activation energy of $\Delta G^{\ddagger}$ = 15.1 kcal/mol at 298 K. Considering all the approximations that had to be made in the calculations (e.g., isolated molecule and neglect of entropic, polarizability and friction effects in the solvent), this value compares remarkably well with the global frequency of circumrotation (72 Hz) recorded[9] at that temperature in C$_2$D$_2$Cl$_4$.

Table 4. Unimolecular Rate Constant Obtained by Applying Transition-State Theory to the Lowest Transition States of Catenane **1**

transition state	T (K)	$\Delta G^{\ddagger}$ (theor)	k (s^{-1})
I$_a$ (perp) -t1	298	12.28	9120
	283	12.25	3100
	258	12.21	390
	253	12.20	245
	248	12.19	151
	243	12.18	91.6
	238	12.17	54.3
I$_b$ (perp) -t3	298	12.50	540000
	283	12.46	208000
	258	12.30	33400
	253	12.26	22200
	248	12.23	14500
	243	12.20	9310
	238	12.16	5870
I$_c$ (perp) -t4	298	12.53	243000
	283	12.54	73200
	258	12.56	7270
	253	12.56	4340
	248	12.56	2530
	243	12.57	1450
	238	12.57	810
II$_a$ (para) -t6	298	4.98	2.54×10^9
	195	4.97	3.28×10^7
	120	4.79	12500
	110	4.78	1940
	105	4.77	673
	100	4.77	210
	95	4.76	57.8
II$_b$ (para) -t8	298	15.09	103
	293	15.07	69.0
	288	15.05	45.6
	283	15.02	29.7
	273	14.98	12.0
	263	14.93	4.53
III (para) -t13	298	11.01	65200
	293	11.01	47000
DRX → GEM	288	11.01	33500
	283	11.01	23500
	273	11.01	11200
	263	11.01	5060
III (para) -t13[a]	298	12.20	9.88
	293	12.24	6.06
GEM → DRX	288	12.29	3.65
	283	12.34	2.16
	273	12.44	0.718
	263	12.54	0.219

[a] Taking the GEM structure as the reactant state.

If one assumes the GEM structure as the global reference, one would obtain a global rate constant of 0.2−0.5 s^{-1}, for an energy barrier (step IIb) of $\Delta G^{\ddagger}$ = 16.1 kca/mol at 298 K. This circumrotation frequency is diminished both by enthalpic effects on the barrier and by a strong increase of the vibrational density of states in the reactant, which, in turn, is due to the presence of a smallest positive eigenvalue of 7.58 cm^{-1} instead of 12.56 cm^{-1}. Since this result would completely underestimate the kinetics of catenane **1** by a factor of 10^3, it ultimately justifies the choice of the XRD structure as the global reference for circumrotation.

Table 4 also shows the calculated rate constant for the interconversion of the XRD and the GEM structures into one another. While this process is likely to occur in the gas phase only, its dynamics is less than 1 order of magnitude slower than the time scale of circumrotation.

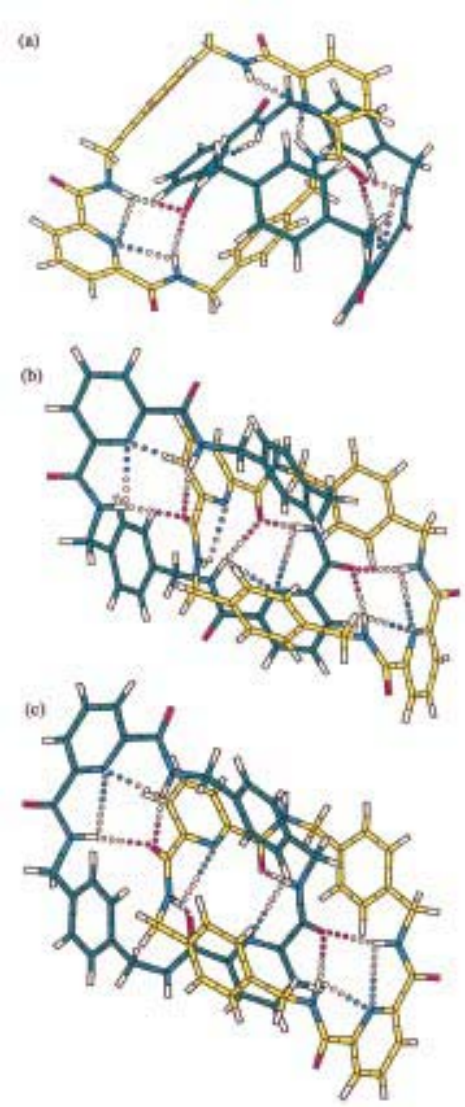

Figure 9. Optimized structures of catenane **2**: (a) the global energy minimum; (b) the second local energy minimum (selected reference); (c) the closest counterpart to the XRD structure of catenane **1**.

The Pyridyl Catenane. (a) Global Minimum and Global Reference. No crystallographic data are yet available for the pyridyl catenane **2**. Starting geometries were therefore derived from the GEM and XRD structures of catenane **1**, as well as all the other 133 structures found for this compound. A simple procedure was set up to substitute pyridine rings for the phenyl groups of the four isophthaloyl moieties. By optimizing the geometry of these structures using the MM3 approach, one obtains 105 different structures of catenane **2**, whose energetics seems again (Figure 6b) largely determined by hydrogen bonding. In comparison with the data displayed for catenane **1** in Figure 6a, hydrogen bonds appear even more dominant in this case.

As with catenane **1**, the GEM of catenane **2** identified by simulated annealing is a rather globular structure (Figure 9a). It can be described as the interlocking of a macrocycle in a boat conformation to a macrocycle in the chair form. This structure has three sets of bifurcated hydrogen bonds and several π-stacks. The next most stable co-conformer (Figure 9b) lies 2.82 kcal/mol above the GEM geometry and closely resembles the XRD structure of catenane **1**. In it, both macrocycles assume chairlike conformations. Once again, the free-energy difference between the two lowest energy structures is reduced to $\Delta G^{\ddagger}(298\ \mathrm{K}) = 1.84$ kcal/mol. Compared with the XRD geometry of **1**, the second most stable structure of **2** requires the inversion of one of the N−H bonds from an orientation "exo" to the cavity of the macrocycle to one that is "endo", so that the corresponding pyridyl-1,3-diamide unit adopts the more favourable cisoid conformation allowing two intramacrocycle N(pyr)···H−N hydrogen bonds.[33] Since this reversal yields an energy stabilization of ~8.44 kcal/mol [this value was estimated by direct comparison with the energy of another structure (Figure 9c) of catenane **2** whose structure is analogous so that of the XRD form of catenane **1**], it strongly affects the energetics and dynamics of circumrotation. In conclusion, by analogy with catenane **1**, the reference structure was taken to be the chair−chair conformation displayed in Figure 9b.

(b) Transition States and Global Energy Profile. Many fewer transition states (Figure 8b) were obtained along the circumrotation paths of catenane **2**, although exactly the same rigid rotation procedure and grid points used for catenane **1** were applied on the selected reference structure. It was soon apparent that most of the states located in the search were 5−6 kcal/mol higher in energy than for **1**. Overall, the entropy decrease at the transition states of **2** (cf. Table 5) are much stronger than those of **1** (cf. Table 3). These observations and the difficulties encountered in getting low-lying transition states corresponding to circumrotational actions can be related to the stronger steric and electrostatic effects that arise due to the four pyridyl rings in this catenane structure.

Although the circumrotation path of catenane **2** was not totally covered, the energy barriers found are sufficient to understand the dynamics of this compound. In general, the transition states of the pyridyl catenane closely resemble those found in the isophthaloyl system. In direct analogy with the conclusions drawn for catenane **1**, the lowest energy pathways (Figure 8b) for the passing of the 1,4-xylyl and pyridyl-1,3-diamide moieties require perpendicular and parallel modes (Figure 10b,c and a,d), respectively. Overall, the foremost structural features of the states associated with the bulkiest groups C_6H_4 (Figure 10c) and C_5H_3N (Figure 10d), are maintained for the passing of the methylene (Figure 10b) and amide (Figure 10a) units. However, the substitution of the phenyl group of the isophthaloyl groups by pyridyl rings has a particularly strong effect on the energy barriers found for the passage of the $CH_2C_6H_4CH_2$ moiety. From the MM3 results shown in Table 5, these appear to require activation energies of 18.6 kcal/mol [$\Delta G^{\ddagger} = 20.5-20.9$ kcal/mol at 298 K], in excellent agreement with the experimental data [$\Delta G^{\ddagger} = 20.5$ kcal/mol at 298 K] obtained from NMR measurements in $C_2D_2Cl_4$.[9]

Three main factors contribute to this higher energy barrier. First, as in the case of catenane **1**, the balance of hydrogen bonds is modified: from the three sets of bifurcated bonds of the minimum structure, one moves to one pair of bifurcated bonds and two regular NH···O bonds in the transition state. Second, a large destabilizing interaction is introduced between the lone pair of a pyridyl nitrogen atom and the core of the passing phenyl group, nicely reflected in the warped shape (Figure 10c) of that phenyl group in the transition state. Third, the presence of an extra endo NH bond in the reference structure increases the barrier as well. This endo NH bond reverses from a cisoid to a transoid conformation, thereby reducing by one the number of N−H···N bridges in the transition state.

(33) (a) Hunter, C. A.; Purvis, D. H. *Angew. Chem., Int. Ed. Engl.* **1992**, *31*, 792−795. (b) Leigh, D. A.; Murphy, A.; Smart, J. P.; Slawin, A. M. Z. *Angew. Chem., Int. Ed. Engl.* **1997**, *36*, 728−732.

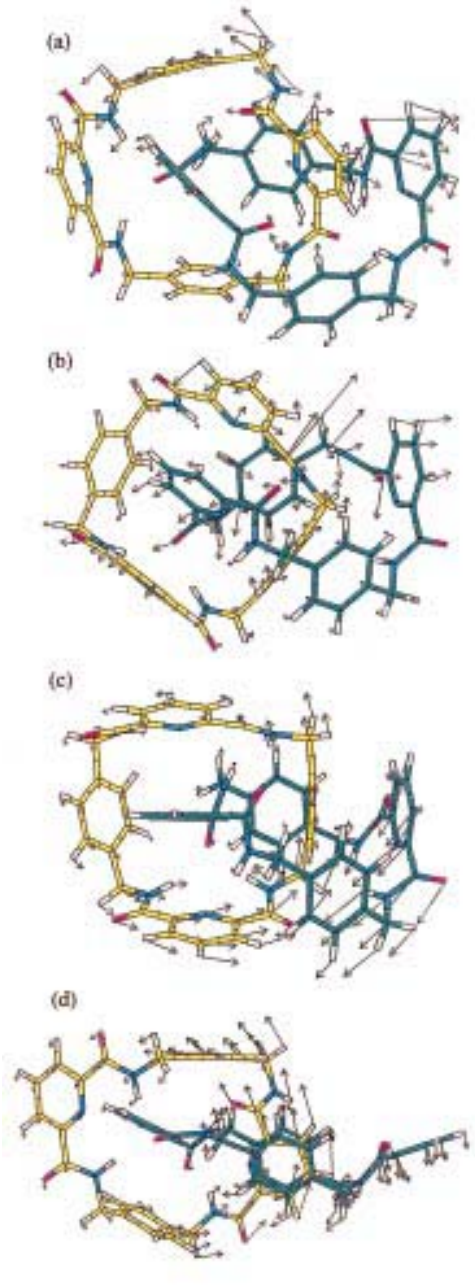

Figure 10. Some of the transition states found along the circumrotation path of catenane **2** for the passage of *p*-xylyl unit in the perpendicular mode (a,b) and of the pyridyl-1,3-diamide unit in the parallel mode (a,d). Mac1 and Mac2 are drawn in yellow and green, respectively. The structures and infinitesimal displacement vectors correspond to the following: (a) step IIa (t7) amide group (*HNOC*−C_5NH_3−CONH); (b) step Ic (t6), methylene group (CH_2−C_6H_4−*CH_2*); (c) step Ib (t4), phenyl group (CH_2−*C_6H_4*−CH_2); (d) step IIb (t10), pyridyl group (HNOC−*C_5NH_3*−CONH).

As with catenane **1**, the parallel mode for the passing of the NH−CO−Ar−CO−NH unit between the two *p*-xylylene moieties of the other macrocycle diminishes the size of the electrostatic and steric barriers to overcome and yields an energy barrier of only 14.8 kcal/mol. This is qualitatively consistent with the observed smaller experimental activation energy of $\Delta G^{\ddagger} = 11.3$ kcal/mol at 298 K in $C_2D_2Cl_4$,[9] although this transition in the isolated catenane seems to be subject to particularly strong vibrational entropic effects: upon their inclusion, in the harmonic approximation, they yield at room temperature a value of $\Delta G^{\ddagger} = 17.4$ kcal/mol. However, one should again bear in mind that the current description does not consider solvation or anharmonic effects and still leaves room for further improvement.

(c) Rate Constants and Dynamics. In view of the higher barriers encountered, the minimum energy circumrotational process for catenane **2** is much slower than in catenane **1**. In contrast to **1**, the rate-determining step for circumrotation in **2** occurs for the passing of the 1,4-xylyl unit (Table 6), a difference in behavior of the two catenanes precisely in agreement with experiment.[5,9] The transition states for **2** give room-temperature rate constants ranging from 6.7×10^{-3} to 1.6×10^{-2} s^{-1} which compare remarkably well with the experimental value of 3×10^{-3} s^{-1} for the global frequency of circumrotation in nonpolar media.[9] In this instance, the C_6H_4 station appears to pass 10−20 times slower than the methylene unit, mostly due to entropic effects on the energy barriers. In spite of their much higher entropic contributions, the passage of the pyridyl rings yields—under the same condition—rate constants comparable to those found for the passing of the isophthaloyl unit of catenane **1** and therefore become a relatively "fast" process for **2**.

Thiophenyl-Based Catenane. (a) Reference Structure. Owing to the smaller size of the five-membered thiophene group, its substitution for phenyl or pyridyl rings tends to produce some large local structural modification and therefore considerable molecular rearrangement after geometry optimization. In this case, an automatic procedure to carry out these substitutions within the structures found previously for catenanes **1** and **2** was deemed inappropriate. We therefore decided to rely on (i) the RR algorithm to generate once again many—51—locally stable confomers from a manually constructed and subsequently optimized reference structure and (ii) the simulated annealing approach to identify the global energy minimum.

The most stable structure (Figure 11) of catenane **3** differs markedly from those found for catenane **1** and catenane **2** in that it tends to favor multipolar electrostatic interactions in a parallel stack containing the four thiophenyl rings at the expense of some hydrogen bonding. The multipolar character of the stacking is directly reflected in the relative disposition of sulfur atoms which display a helicoidal pattern. Correspondingly, hydrogen bonding is globally weaker and has a reduced influence on the energetics of this catenane (Figure 12). From this structural feature one can deduce a lower dependence of the kinetics of circumrotation on the solvent polarity, as found experimentally.[9]

Although the global minimum is again made up of one macrocycle in the chair conformation and one macrocycle in the boat conformation, its energy appears to be less sensitive to vibrational entropic effects then the other two catenanes. This is probably due to a reduction of steric interactions caused by the smaller size of the thiophene rings and to the reduced role of hydrogen bonds in the structure. In contrast with catenanes **1** and **2**, inclusion of entropic effects does not modify significantly the energy difference with the next most stable conformer: from the MM3 value of 2.56 kcal/mol, one gets a free-energy difference of 2.15 kcal/mol at room temperature.

Since the overall aspect of the GEM structure is not as compact as those of the first two catenanes, an observation substantiated by the similar role of entropy in their two most stable structures, this time it therefore seemed reasonable to select the GEM structure as the reference for circumrotational actions.

(b) A Plethora of Transition States. As many as 37 transition states were obtained from catenane **3**, from a set of

Table 5. Transition States Found along the Circumrotation Path of the Pyridyl-Based Catenane **2**

obsd passing[a]	$\Delta U^{\ddagger}$ (kcal/mol)	$\Delta U^{\ddagger}$ $1/2\Sigma(\Delta\omega_i)$ (kcal/mol)	$\Delta S^{\ddagger}$ (cal/(mol K))	ω (i cm^{-1})	M^*	K^*
I_b (para) -t1	39.37	37.33	−13.56	16.04	7.12	-1.83×10^3
I_b (para) -t2	31.32	28.88	+1.53	29.54	7.80	-6.80×10^3
I_b (perp) -t3	19.19	18.33	−8.64	23.53	6.44	-3.56×10^3
I_b (perp) -t4	18.60	17.57	−9.77	30.58	7.89	-7.38×10^3
I_c (para) -t5	36.29	34.11	−2.68	15.19	7.12	-1.64×10^4
I_c (perp) -t6	18.55	17.40	−5.81	33.35	8.49	-9.94×10^4
II_a (perp) -t7	12.27	12.58	−15.63	38.75	8.52	-1.28×10^4
II_b (perp) -t8	19.05	18.11	−7.94	10.18	6.79	-7.03×10^2
II_b (para) -t9	17.66	17.0	−1.76	12.53	6.91	-1.09×10^3
II_b (para) -t10	14.82	14.11	−12.7	16.49	7.49	-2.03×10^3
II_c (perp) -t11	22.92	21.75	−6.79	19.18	7.05	-2.59×10^3
II_c (perp) -t12	20.28	20.16	−13.42	28.20	7.97	-6.34×10^3

[a] I_a, methylene unit; I_b, phenyl unit of the 1,4-*p*-xylyl moiety; II_a, amide unit; II_b, thiophenyl unit of the NHCO−C_5NH_5−CONH moiety.

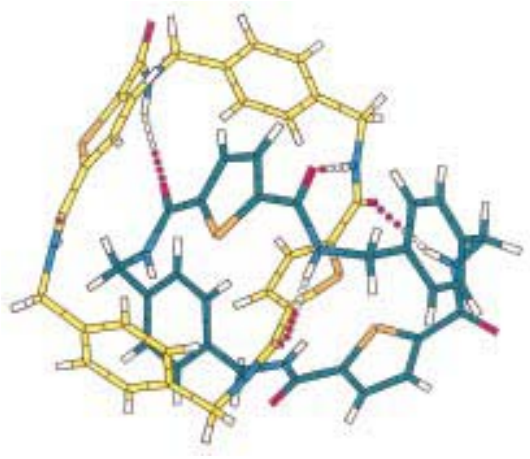

Figure 11. The global energy minimum of the thiophenyl catenane **3**.

Table 6. Unimolecular Rate Constant Obtained by Applying Transition-State Theory to the Lowest Transition States of Catenanes **2**

transition state	T (K)	$\Delta G^{\ddagger}$(theor)	k (s^{-1})
I_b (perp) -t3	373	21.55	3.46
	368	21.50	2.47
	363	21.46	1.75
	360	21.44	1.41
	298	20.90	0.00667
I_b (perp) -t4	373	21.21	6.22
	368	21.16	4.51
	363	21.11	3.23
	360	21.09	2.64
	298	20.48	0.0158
I_c (perp) -t6	373	19.60	53.3
	368	19.53	38.7
	363	19.51	27.8
	360	19.49	22.7
	298	19.13	0.137
II_a (para) -t7	298	17.23	6.57
	238	16.30	0.0359
	235	16.25	0.0258
	233	16.22	0.0206
	230	16.17	0.0146
II_b (para) -t10	298	17.89	54.9
	238	17.10	0.126
	235	17.09	0.0859
	233	17.07	0.0661
	230	17.03	0.0442

795 zeroth-order structures generated using a rigid rotation chart of 1280 points ($-180° \le \theta \le 180°$; $-90° \le \phi \le 30°$). They cover an energy range of more than 20 kcal/mol and reflect the less-sterically demanding character and the high flexibility of this molecule whose transition states exhibit a very versatile behavior of the passing unit (both perpendicular and parallel modes were found for each fragment). At odds with that calculated for the other catenanes, this molecule shows an increase in the vibrational entropy at the transition states (Table 7), a feature that one can relate to a partial or complete disruption of the multipolar interactions that hold together the quadruple-decker sandwich of thiophene rings in the reference structure.

The transition states found (Figure 12) along the lowest energy paths for circumrotation of the thiophene catenane resemble closely those of the isophthaloyl one, with a perpendicular mode of π-stacks for the passing of the $CH_2C_6H_4CH_2$ moiety (Figure 12b), and a parallel or "sandwich" mode for the passing of the NH−CO−C_4H_2S−CO−NH fragment (Figure 12d). The parallel transition structures are very similar to the reference structure because of the presence of a triple- or quadruple-decker sandwich of thiophene rings which display, again, a helicoidal pattern for the location of sulfur atoms. Unsurprisingly, this passing requires very low activation energies (5−8 kcal/mol) for both the NHCO and the C_4H_2S units.

In this case, NMR measurements in $C_2D_2Cl_4$ could detect only one energy barrier because they are so small.[9] The theoretical data displayed in Table 7 suggest that this corresponds to the passage of the $CH_2-C_6H_4-CH_2$ moiety (Figure 12a,b). As with catenane **2**, the most favorable perpendicular mode implies that the lone pair of a sulfur atom points directly toward the core of the passing phenyl group. However, the larger size of the macrocyclic cavities helps to limit the destabilizing effects of this interaction. Furthermore, reversal of the thiophenyl-1,3-diamides from cisoid and transoid conformations was not observed. These effects, along with the reduced role of hydrogen bonding, diminish the height of the energy barriers. Upon inclusion of vibrational enthalpic and entropic effects, the lowest transition state found for the passing of a methylene unit lies at $\Delta G^{\ddagger}(298\ K) = 11.9$ kcal/mol above the reference geometry, which compares very well with an experimental value of 11.6 kcal/mol. The first two transition states found for the phenyl-exchange station also fit fairly well with experiment, as they require an activation energy of 10.5 and 11.2 kcal/mol at room temperature.

(c) Rate Constants and Dynamics. Inspection of the results reported in Table 8 prompts two comments: the first relates to the inversion of barriers and rate constants for the passing of a phenyl group (step Ib). The rate constant associated with the transition state identified by a $\Delta G^{\ddagger}(298\ K) = 10.52$ kcal/mol is 22 times smaller than the rate constant associated with a second transition state identified by $\Delta G^{\ddagger}(298\ K) = 11.22$ kcal/mol. From the point of view of rearrangement efficiency this is therefore the state to consider for passing that unit, which incidentally improves the agreement between experiment and

Table 7. Transition States Found along the Circumrotation Path of the Thiophenyl-Based Catenane **3**

IIb	$\Delta U^{\ddagger}$ (kcal/mol)	$\Delta U^{\ddagger}$ $1/2\Sigma(\Delta\omega_i)$ (kcal/mol)	$\Delta S^{\ddagger}$ (cal/(mol K))	ω (i cm^{-1})	M^*	K*
I_a (para) -t1	24.70	23.30	+10.38	27.06	6.97	-5.10×10^3
I_a (perp) -t2	17.37	16.03	−1.34	27.66	8.95	-6.85×10^3
I_a (perp) -t3	14.38	13.19	+4.33	21.88	7.69	-3.68×10^3
I_b (perp) -t4	13.91	12.94	−1.91	26.60	7.99	-5.65×10^3
I_b (perp) -t5	12.90	11.86	+2.15	10.75	7.42	-8.58×10^2
I_b (perp) -t6	11.95	11.09	+1.90	10.67	7.73	-8.82×10^2
II_a (para) -t7	27.38	25.77	+4.53	30.53	6.97	-6.50×10^3
II_a (para) -t8	26.37	24.46	+9.36	51.01	7.38	-1.92×10^4
II_a ( ) -t9	22.80	21.83	+4.87	12.78	8.37	-1.37×10^3
II_a (para) -t10	22.45	21.29	+6.83	40.55	8.58	-1.41×10^4
II_a ( ) -t11	19.28	17.53	+14.00	14.66	7.33	-1.57×10^3
II_a (perp) -t12	17.65	15.87	+5.56	13.85	7.82	-1.50×10^3
II_a (para) -t13	15.36	13.29	+3.04	44.55	8.20	-1.63×10^4
II_a (para) -t14	14.83	12.65	+10.47	34.05	7.95	-9.22×10^3
II_a (para) -t15	13.45	12.18	+6.96	11.64	8.18	-1.11×10^3
II_a (para) -t16	10.73	9.05	+3.84	65.18	7.80	-3.30×10^4
II_a (para) -t17	9.24	8.68	+4.02	13.96	7.80	-1.52×10^3
II_a (para) -t18	8.29	7.43	+6.21	21.15	7.47	-3.30×10^3
II_a ( ) -t19	8.26	6.86	+4.67	23.64	7.87	-4.39×10^3
II_b ( ) -t20	24.64	22.78	+4.29	45.45	8.29	-1.71×10^4
II_b ( ) -t21	23.36	21.68	−2.80	19.11	7.97	-2.91×10^3
II_b (perp) -t22	19.86	19.16	+4.32	19.94	8.25	-3.28×10^3
II_b ( ) -t23	19.28	17.53	+14.00	14.66	7.32	-1.57×10^3
II_b (para) -t24	16.85	15.53	+6.62	12.78	7.97	-8.43×10^3
II_b (para) -t25	16.50	15.01	+10.42	11.17	7.84	-9.78×10^2
II_b (para) -t26	16.30	15.16	+6.17	26.75	6.71	-4.80×10^3
II_b ( ) -t27	15.06	13.8	+4.43	15.76	7.02	-1.74×10^3
II_b (perp) -t28	14.78	13.46	−1.99	22.48	8.51	-4.30×10^3
II_b (para) -t29	13.47	12.17	+8.34	24.80	7.70	-4.74×10^3
II_b (para) -t30	12.30	11.09	−2.34	30.59	7.12	-6.67×10^3
II_b (perp) -t31	11.50	10.47	+7.45	27.29	8.30	-6.18×10^3
II_b (para) -t32	10.06	9.12	+3.72	24.81	7.17	-4.42×10^3
II_a (perp) -t33	8.96	8.60	−3.30	24.18	7.20	-4.21×10^3
II_b (para) -t34	5.17	4.46	−0.06	7.67	7.96	-4.68×10^2
II_b (para) -t35	5.28	5.01	−12.12	32.64	9.021	-9.62×10^3
II_b (para) -t36	5.42	5.28	+0.23	37.91	7.60	-1.10×10^4
II_b (para) -t37	5.42	4.7	+1.53	33.51	9.26	-1.04×10^4

[a] I_a, methylene unit; I_b, phenyl unit of the *p*-xylyl moiety; II_a, amide unit; II_b, thiophenyl unit of the NHCO−C_5SH_4−CONH moiety.

theory. However, with values of the order of 3.5×10^6 s^{-1}, the associated rate constants appear to overshoot completely the experimental value of 9600 Hz found for the frequency of circumvolution of catenane **3** in nonpolar conditons.[9]

The second comment relates to the identification of the rate-determining step which, in analogy with catenane **1**, corresponds to the passage of the methylene unit. Its rate constant is found to be 2 orders of magnitudes smaller than the passing of the bulkier phenyl groups. This yields an overall frequency of circumrotation of 12 400 Hz, in excellent agreement with experiment.

Conclusions

The circumrotations of the interlocked macrocyclic components of benzylic amide catenanes (containing phenyl, pyridyl, and thiophenyl-1,3-dicarbonyl aromatic rings) are highly concerted processes which require considerable molecular arrangements to accommodate the partial disruption of the internal networks of hydrogen bonds and minimize energy barriers. Along the minimum energy circumrotational pathways, the catenanes resort to the use of many stabilizing effects such as the formation of π-stacks, phenyl−phenyl T-shape or herringbone complexes, and partial amide bond rotamerization. These conformational and co-conformational rearrangements may have positive or—at least in the pyridyl case—negative effects on the energetics and dynamics of circumrotation. In spite of this complexity, and therefore quite remarkably, the catenanes adopt common motifs and patterns of response during the passing of particular sections through their macrocyclic cavities. In practice, their behavior can be rationalized using the specific nomenclature introduced in the discussion section which describes in a natural manner the foremost structural features of the transition states and implicitly identifies some of the key π-stacking interactions as important stabilizing influences in these states. The passage of a 1,4-xylyl fragment always occurs in the so-called perpendicular mode, whereas the passing of the isophthaloyl, pyridyl-1,3-dicarbonyl, or thiophenyl-1,3-dicarbonyl moieties proceeds via a parallel transition state. The steric constraints of the process make these common qualitative features independent of the force field. Although this study illustrates the impracticality of a complete investigation of the very large number of degrees of freedom of the potential energy surfaces of these molecules, the present characterization and the overall truly remarkable qualitative and quantitative agreement with experiment, in terms of both activation energies and rate constants, makes us believe that we have consistently captured the nature of macrocycle circumvolution in benzylic amide catenanes. A word of caution needs to be added because our simulations use the isolated molecule approximation while the NMR experiments were performed in $C_2D_2Cl_4$, a solvent, however, that does not disrupt the hydrogen bond system and

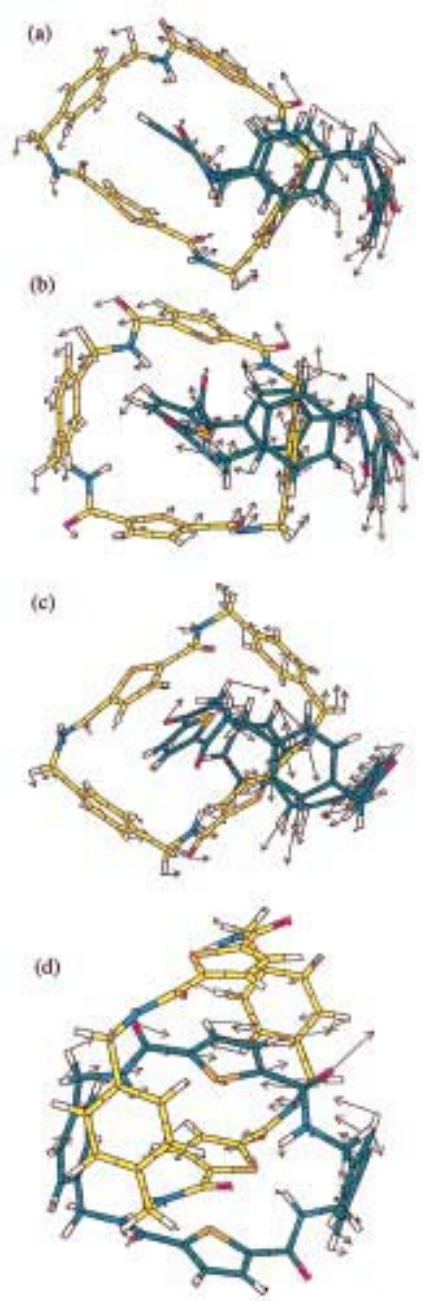

Figure 12. Some of the transition states found along the lowest energy circumrotation paths of catenane **3**: (a) step Ia (t3), methylene group; (b) step Ib (t6), phenyl group; (c) step IIa, amide group (t19); (d) step IIb, thiophenyl group (t35). Mac1 and Mac2 are drawn in yellow and green, respectively.

cannot force itself inside the macrocyclic cavities where the predominant structural rearrangements take place.

In spite of the crude approximations of the present treatment, molecular mechanics affords a complete qualitative, or even semiquantitative, understanding of the energetics and dynamics of these complicated molecular systems. One possible reason for the success lies in the mechanism of the circumrotation, when entails a continuous breaking and reconstruction of the intramolecular inter-ring network of hydrogen bonds and π-stacks, phenomena for which molecular mechanics is parameterized. It is worth mentioning that the particular force field used, namely, MM3, has been further validated for the study of minimum energy structures of catenanes, in recent work

Table 8. Unimolecular Rate Constants Obtained by Applying Transition-State Theory to the Lowest Transition States of Catenane **3**

transition state	T (K)	$\Delta G^{\ddagger}$(theor)	k (s^{-1})
I_a (perp) -t3	298	11.90	12400
	272	12.01	1340
	262	12.06	507
	252	12.10	178
	242	12.14	57.2
	232	12.18	16.7
	230	12.19	12.9
	225	12.21	6.63
	222	12.23	4.38
	220	12.24	3.30
I_b (perp) -t4	298	13.51	65000
	272	13.45	7290
	262	13.44	2800
	252	13.42	999
	242	13.40	328
	232	13.38	97.6
	230	13.38	75.5
	225	13.37	39.3
	222	13.36	26.1
	220	13.36	19.8
I_b (perp) -t5	298	11.22	3.52×10^6
	272	11.27	459000
	262	11.30	189000
	252	11.32	72300
	242	11.34	25600
	232	11.36	8310
	230	11.37	6550
	225	11.38	3560
	222	11.38	2440
	220	11.39	1880
I_b (perp) -t6	298	10.52	160000
	272	10.57	24700
	262	10.59	11000
	252	10.61	4550
	242	10.63	17.60
	232	10.65	626
	230	10.65	504
	225	10.66	288
	222	10.67	203
	220	10.67	161
II_a ( ) -t19	298	5.47	6.44×10^8
	195	5.96	8.75×10^5
	130	6.25	72.1
	125	6.28	23.5
	120	6.30	6.98
	115	6.32	1.87
	110	6.35	0.445
II_b (para) -t35	298	8.62	4.50×10^8
	272	8.30	1.99×10^8
	262	8.19	1.39×10^8
	252	8.06	9.43×10^7
	242	7.94	6.21×10^7
	232	7.82	3.94×10^7
	195	7.37	4.89×10^6
	130	6.59	7080
	125	6.53	3230
	120	6.46	1380
	115	6.40	549
	110	6.34	201
II_b (para) -t36	298	5.21	1.82×10^9
	195	5.24	1.30×10^7
	120	5.25	1790
	110	5.25	221
	100	5.26	17.9
	90	5.26	0.837
II_b (para) -t37	298	4.24	7.80×10^9
	195	4.40	8.88×10^7
	120	4.52	29700
	110	4.53	4520
	100	4.55	475
	90	4.56	304

carried out on the inelastic neutron scattering spectra of CAT1.[34] It should also be emphasized that our analysis for CAT1 is based on the assumption that the XRD structure is the reference of the process. This assumption is justified by some experimental evidence (for instance, recrystallization from various solvents consistently affords the same crystal structure) and by theoretical considerations (see text).

The shape of the transition states furnishes a simple explanation of the large differences observed in the NMR experiments. For instance, the increase by 5-6 kcal/mol of the barrier from the isophthaloyl to the pyridyl catenane for the *p*xylyl unit is caused by the combined effect of depriving the system of a stabilizing phenyl−phenyl T-shape interaction and replacing it by the destabilizing interaction between two negatively charged centers plus a steric effect that forces a pyridyl-1,3-diamide group from a cisoid to a transoid conformation in the transition state. As a second example, in the thiophene catenane the low barriers to circumrotation are largely a result of the release of the destabilizing interactions caused by the presence of the smaller five-membered rings, which enlarge the macrocyclic cavity, and the weakening of hydrogen bonds at the benefit of cooperative multipolar interactions in stacks of thiophene rings.

The consideration of dynamic effects, by means of transition-state theory, highlights the complexity of these processes and provides some unexpected insights. Contrary to what might be assumed intuitively, the rate-determining steps do not necessarily correspond to the passage of the bulkiest groups through the cavities. The structures of the transition states, and their chaotic behavior upon relaxation, indicate that circumrotation of one ring induces—or synergistically eases—rotation of the other. The assignment of the origin of the energy barriers, the characterization of the structures and intercomponent interactions in the transition states and local intermediates, and the suggestion of a cooperative rotation mechanism thus provides us with our first significant understanding of circumrotational phenomena in a mechanically interlocked molecular system.

While there is still clearly room for improvement in the modeling by including, among other things, solvent polarization, entropic and friction effects, or mimicking the highly modified nature of the circumrotation in strongly polar solvents, the most challenging problem to be addressed in the near future concerns the circumrotation of catenanes in crystalline solids, thin films, and on surfaces[35]—the forms in which these remarkable molecular architectures are most likely to be exploited. Experimental and theoretical investigation of these complex motions in condensed phases is a mandatory step for the practical development of catenane-based materials.

Acknowledgment. We thank Aden Murphy for his patience and assistance with the color pictures. This work was supported by the European Community under TMR Contract FMRX-CT96-0059, a European Network on Benzylic Amide Catenanes (ENBAC). M.S.D. was the recipient of a one-year TMR-ENBAC scholarship in Bologna. He is grateful to the FWA_Vlaanderen, the science foundation of Flanders (Belgium), for his position as a senior research assistant at the Limburgs Universitair Centrum. F.Z. received partial financial support from MURST project “Supramolecular devices”.

JA9815273

(34) Caciuffo, R.; Degli Esposti, A.; Deleuze, M. S.; Leigh, D. A.; Murphy, A.; Paci, B.; Parker, S. F.; Zerbetto, F. *J. Chem. Phys.* **1998**, *109*, 11094.

(35) Deleuze, M. S.; Leigh, D. A.; Zerbetto, F., in preparation.